On the physics of upgradient momentum transport in unstable eastward jets

Henk A. Dijkstra and Paul C.F. van der Vaart

Institute for Marine & Atmospheric research Utrecht

Department of Physics & Astronomy

Utrecht University

Utrecht, The Netherlands

Running Title: Upgradient momentum transport in unstable jets

Keywords: Baroclinic/barotropic instability, momentum transport

Corresponding Author:

Henk A. Dijkstra

Institute for Marine and Atmospheric research Utrecht

Department of Physics and Astronomy

Utrecht University

Princetonplein 5, 3584 CC Utrecht

The Netherlands

Phone: -31-30-2533276; Fax: -31-30-2543163

email: dijkstra@fys.ruu.nl

Abstract

The weakly nonlinear finite amplitude evolution of mixed baroclinic / barotropic instabilities of an eastward zonal jet is considered in a two-layer QG-model on a midlatitude beta-plane. Linear friction is included and is essential to the momentum transport. The focus is two parameter regimes, one corresponding to the Gulf Stream and the other to the Antarctic Circumpolar Current. In the latter case, the nonlinear self-interaction of the most unstable mode causes upgradient momentum transport and therefore sharpens the jet. The analysis of this example leads to a clear description of the physics of this process. It also indicates why upgradient momentum transport does not occur in the Gulf Stream regime.

1 Introduction

An intriguing problem in physical oceanography is the physics of the maintenance of zonal jets. It is well-known that these zonal jets are susceptible to instabilities, which can be both of baroclinic and barotropic nature. During the instability process, energy is transferred from the zonal jet to the disturbances which propagate out of regions of strong mean flow. One would expect that these jets broaden and eventually decay in the presence of friction. As zonal jets appear as pronounced permanent features, this raises the question how they are maintained.

An example of such an eastward jet is the Antarctic Circumpolar Current (ACC). The ACC is a permanent feature in the Southern Ocean and both observations Nowlin and Klinck (1986) and numerical studies (McWilliams *et al.*, 1978; Marshall *et al.*, 1993) have provided a characterization of the dynamical balances of this current. The momentum input by the wind stress is concentrated horizontally in a few narrow jets by the high eddy activity in the upper ocean, it is transported downward by isopycnal form stress and removed at the bottom by topographic form stress. This eddy activity is caused by the high degree of instability of the mean zonal current, which strongly meanders. Observed eddies have a diameter of $60 - 200$ $[km]$ and swirl velocities are in the order of 0.5 $[ms^{-1}]$.

The instability characteristics of the ACC and the resulting energy and momentum transfer were studied within a two-layer quasi-geostrophic ocean

model by McWilliams *et al.* (1978). For the flow in a periodic channel (case CH in their paper), they find that energy is transferred from the mean state to the perturbations due to instability. Due to the interactions of the perturbations, zonal momentum is transferred from regions of small to regions of large mean jet velocity leading to a sharper jet profile. By a careful budget analysis, they identify the physical processes which induce this momentum transfer. However, in these budget analyses it is difficult to obtain a mechanistic picture of how this upgradient momentum transfer is accomplished. The mean state is far above criticality and many different unstable modes contribute to the total momentum budget.

Although several other effects may contribute to the maintanance of zonal jets (e.g. diabatic processes (Hoskins and Valdes, 1990)), upgradient momentum transfer is certainly important. To explain the momentum transfer due to instabilitities of a zonal jet, one often refers to Kuo (1951) and Held (1975). The classical result as given in Kuo (1951) for the inviscid barotropic instability of an eastward jet, with steady zonal velocity $\overline{u}$ is that

$$\frac{\partial u}{\partial t} = -C\ \lambda\ \frac{\partial \overline{\Pi}}{\partial y} \tag{1a}$$

where u is the total zonally averaged velocity and λ is the growth factor of the perturbations, $\frac{\partial \overline{\Pi}}{\partial y} = \beta - \frac{d^2\overline{u}}{dy^2}$ is the potential vorticity gradient of the zonal jet and C is a positive function of the meridional coordinate y. Hence, unstable modes on the zonal jet ($\lambda > 0$) transport westerly momentum out of the region where the basic state potential vorticity gradient is positive

into the region where this quantity is negative. The consequence is that for an eastward jet, with typically positive $\frac{\partial \Pi}{\partial y}$ at its core, the instabilities tend to weaken the jet and growing barotropic disturbances will transport momentum downgradient.

Held (1975) extends the analysis of Kuo (1951) for the case of instabilities in a two-layer quasi-geostrophic model. The generalization of (1a) in this model becomes

$$\frac{\partial u}{\partial t} = -\lambda \left(C_1 \frac{\partial \overline{\Pi}_1}{\partial y} + C_2 \frac{\partial \overline{\Pi}_2}{\partial y}\right) \tag{1b}$$

where u is now the depth averaged velocity, $\frac{\partial \overline{\Pi}_i}{\partial y} = \beta - \frac{d^2 \overline{u}_i}{dy^2} + (-1)^i (\overline{u}_2 - \overline{u}_1)/R^2$ the potential vorticity gradient, R the internal Rossby deformation radius and both C_1 and C_2 are positive functions of y. From (1b), it also follows that unstable modes transport momentum out of the region where the basic state potential vorticity gradient is positive. There may be cases for which $\frac{\partial \overline{\Pi}_1}{\partial y} > 0$ and still upgradient momentum transfer occurs, for example when $\frac{\partial \overline{\Pi}_2}{\partial y}$ is strongly negative.

The analyses of Kuo (1951) and Held (1975) are unsatisfactory because in both studies, solutions of the linear stability problem are used to monitor the magnitude of the momentum transfer. Since the amplitude of the perturbations is arbitrary, the magnitude of the induced momentum transfer is undetermined. Using Lagrangian concepts, the relation (1b) has been

generalized in Rhines and Holland (1979) to

$$\frac{\partial u}{\partial t} = -(C_1\kappa_1\frac{\partial\overline{\Pi}_1}{\partial y} + C_2\kappa_2\frac{\partial\overline{\Pi}_2}{\partial y}) \tag{1c}$$

For each layer j, κ_j is the $\kappa^{(22)}$ component of the Lagrangian diffusivity tensor κ in the horizontal plane which is a kinematic quantity measuring the dispersion of fluid parcels due to north-south movement of the perturbations. As mentioned by Rhines and Holland (1979), similar conclusions can be drawn from (1c) as from (1b) without reference to linear stability theory, since $\kappa_j > 0$ in the case of instability. However, to determine the amplitude, one is faced with a closure problem on the κ_j which is not easily solved.

To determine the strength of the momentum transfer, one has to consider the interactions which arise through the finite amplitude development of the instabilities. The study of these interactions in unstable zonal jets was pioneered by Pedlosky (1970) in the two-layer quasi-geostrophic context. In the weakly nonlinear regime, the slightly supercritical conditions in a particular parameter, say the vertical shear, are measured by a parameter ε. The nonlinear self-interaction of the most unstable mode (see e.g. Eckhaus (1965)) leads to a modification of the basic zonal jet through an advective potential vorticity flux at $\mathcal{O}(\varepsilon^2)$ which is measured in each layer by

$$Re(J(\phi_j, q_j^*)) = Re(\frac{\partial\phi_j}{\partial x}\frac{\partial q_j^*}{\partial y} - \frac{\partial\phi_j}{\partial y}\frac{\partial q_j^*}{\partial x}) \tag{1d}$$

where ϕ_j is the perturbation streamfunction, q_j its potential vorticity and the superscript * indicates complex conjugate. The quantities are evaluated

at criticality and Re indicates the real part.

In the classical inviscid baroclinic instability problem, with constant jet velocity in each layer, it follows that $Re(J(\phi_j, q_j^*)) = 0$, since at criticality the potential vorticity is a real multiple of the streamfunction in each layer (Pedlosky, 1963, 1970). Also for the inviscid barotropic instability problem of an arbitrary jet profile, the right hand side of (1d) is exactly zero for the same reason. In both cases, a non-zero contribution to the advective potential vorticity flux is generated at $\mathcal{O}(\varepsilon^3)$, but upgradient momentum transport does not occur. When $\mathcal{O}(1)$ linear friction is included in both classical cases, the potential vorticity is no longer a real function of the streamfunction at criticality giving a potential vorticity flux (1d) at $\mathcal{O}(\varepsilon^2)$. However, even in this case it is found that the momentum transport is always downgradient (Romea, 1977; Pedlosky, 1987, e.g.).

A mixed barotropic/baroclinic instability is necessary for upgradient momentum transfer (Pedlosky, 1987). In that case, the linear stability problem cannot be solved analytically anymore, which complicates the determination of the finite amplitude evolution. In Van der Vaart and Dijkstra (1997), referred to as VD97 hereafter, this problem was solved numerically and focus was on secondary (sideband) instabilities using Ginzburg-Landau theory. For a jet in a Gulf Stream (GS) parameter regime the momentum transfer is found to be downgradient, even in case of mixed instabilities.

In this paper, we focus on a parameter regime relevant to the ACC using

the same two-layer quasi-geostrophic model in a β-plane channel as in VD97. The simplest case of $\mathcal{O}(1)$ friction is considered and an example is given of upgradient momentum transfer due to the finite amplitude development of mixed instabilities. Nonlinear interactions between perturbations induce the upgradient momentum transport while the amplitude of the transport is determined by the nonlinear equilibration of the instability. The physics of how the nonlinear self-interaction of the most unstable mode is able to establish this transport is described in terms of the decomposition of the potential vorticity flux ($1d$) into interfacial form drag and Reynolds stresses. By following a path from the ACC-regime to the GS-regime a transition in transport of momentum is found and the mechanical energy balances are used to characterize this boundary. The results serve as an example of the more abstract results in Rhines and Holland (1979) and make the physical description from the budget analyses as in McWilliams *et al.* (1978) much more explicit.

2 Methods

2.1 Model

A zonal channel of width L, situated on a midlatitude β-plane, and with constant depth D contains a two-layer ocean with densities ρ_1 and ρ_2, reduced gravity $g' = g(\rho_2 - \rho_1)/\rho_1$ and mean layer thicknesses H_1 and H_2 ($D =$

$H_1 + H_2$). Within a quasi-geostrophic model (Pedlosky, 1987), we consider the stability of a zonal jet of the form

$$\overline{u}_1(y;\nu) = \frac{sech^2(\frac{y}{\nu}) - sech^2(\frac{1}{\nu})}{sech^2(\frac{1}{\nu})} \quad ; \quad \overline{u}_2(y) = \alpha\overline{u}_1(y;\nu) \tag{2}$$

such that $\overline{u}_1(-1;\nu) = \overline{u}_1(1;\nu) = 0$. The parameters α and ν measure the relative strength of the jet in the lower layer and the width of the jet, respectively. For a value $\nu = 0.5$, the zonal velocity profile $\overline{u}_1$ is plotted in Fig. 1.

With the usual quasi-geostrophic scaling, the equations for the perturbations on the basic state (2) are written in terms of the perturbation streamfunctions ϕ_j in both layers, i.e.

$$\begin{cases} (\frac{\partial}{\partial t} + \overline{u}_1\frac{\partial}{\partial x})q_1 + \overline{\Pi}_1'\frac{\partial\phi_1}{\partial x} + J(\phi_1, q_1) + r\nabla^2\phi_1 = 0 \\ (\frac{\partial}{\partial t} + \overline{u}_2\frac{\partial}{\partial x})q_2 + \overline{\Pi}_2'\frac{\partial\phi_2}{\partial x} + J(\phi_2, q_2) + r\nabla^2\phi_2 = 0. \end{cases} \tag{3a}$$

The Jacobian J, given by

$$J(\phi_j, q_j) = \frac{\partial\phi_j}{\partial x}\frac{\partial q_j}{\partial y} - \frac{\partial\phi_j}{\partial y}\frac{\partial q_j}{\partial x} \tag{3b}$$

contains all nonlinear interactions of the perturbations. The potential vorticity q_j in both layers is given by

$$q_1 = \nabla^2\phi_1 - F(\phi_1 - \phi_2) \quad , \quad q_2 = \nabla^2\phi_2 + \delta F(\phi_1 - \phi_2) \tag{3c}$$

and the gradient of potential vorticity of the basic state by

$$\overline{\Pi}_1'(y) = \beta + F(1-\alpha)\overline{u}_1 - \frac{d^2\overline{u}_1}{dy^2} \tag{3d}$$

$$\overline{\Pi}_2'(y) = \beta - \delta F(1-\alpha)\overline{u}_1 - \frac{d^2\overline{u}_2}{dy^2} \tag{3e}$$

The equations contain the following parameters, the strength of the planetary vorticity gradient β, the rotational Froude number F and the layer thickness ratio δ. These parameters are defined as

$$\beta = \frac{\beta_0 L^2}{U} \qquad F = \frac{f_0^2 L^2}{g' H_1} \qquad \delta = \frac{H_1}{H_2} \tag{4}$$

Furthermore, linear friction is taken into account in both layers through a dimensionless friction coefficient r (Pedlosky, 1987). The dimensional value of the friction coefficient in the lower layer is taken four times larger than that in the upper layer, but since the lower layer has a much larger depth, this yields similar values for the dimensionless friction in both layers. These equations are complemented with boundary conditions at the channel walls ($y = \pm 1$) in both layers

$$\frac{\partial \phi_j}{\partial x} = 0 \tag{5a}$$

corresponding to the kinematic condition of no normal flow at the channel walls at $\mathcal{O}(1)$ in the quasi-geostrophic approximation. Also the meridional velocity at the next order in the Rossby number expansion has to vanish, but although this velocity does not appear in the equations, the boundary condition at $y = \pm 1$ can be formulated as

$$\lim_{l \to \infty} \frac{1}{l} \int_{-l}^{l} \frac{\partial^2 \phi_j}{\partial y \partial t} \, dx = 0 \tag{5b}$$

where l is a zonal averaging interval.

Standard parameters corresponding to the ACC-regime are shown in Table 1. These parameters have similar values as in the study of McWilliams

et al. (1978). Also the values of the GS-regime are shown for which both β and F are different by an order of magnitude, compared to the ACC regime. Note that the values of ν and r are slightly different from those used in VD97. The potential vorticity gradient of the jet in each layer, for the ACC case, is plotted in Fig 2. Although $\frac{d\overline{\Pi}_2}{dy}$ is slightly negative only over a small interval, the jet satisfies the inviscid necessary condition of instability (as derived from e.g. (1b)) and indeed the inviscid jet can be shown to be unstable using the methods below.

2.2 Linear stability analysis

To determine sufficient conditions for instability of the basic state (2), the governing equations are linearized in the amplitude of the perturbations. The resulting system of equations allows for traveling wave solutions in the x - direction with wavenumber k, complex growth factor σ and unknown meridional structure, i.e.

$$\Phi(x, y, t) = \Psi(y)e^{ikx+\sigma t} + c.c. \tag{6a}$$

where $\Psi = (\phi_1, \phi_2)^T$ and $c.c.$ indicates complex conjugates. The eigenvalue σ is written as $\sigma = \lambda + i\omega$ and considered as a function of the wavenumber k and a control parameter, say μ, of the system. If $\lambda > 0$ for a particular wavenumber k, the basic state is unstable. The neutral curve, $\lambda(k, \mu) = 0$ in the (k, μ) plane separates linearly stable basic states from unstable ones.

As control parameter, $\mu = \beta^{-1}$ is chosen and the linear friction coefficient r is fixed. The neutral curve in the (k, β^{-1}) plane is shown in Fig. 3 and has a minimum at (k_c, μ_c), the critical values, at which

$$\lambda(k_c, \mu_c) = 0, \ \frac{\partial \lambda}{\partial k}(k_c, \mu_c) = 0, \ \frac{\partial^2 \lambda}{\partial k^2}(k_c, \mu_c) < 0 \tag{6b}$$

Critical values occur at $\beta_c = 48.90$ and $k_c = 11.37$, the latter corresponding to a wavelength of 540 km. The internal Rossby deformation radius of the two-layer model $L_R = \frac{g' H_1}{f_0^2 (1+\delta)}$ is about 48 km. The horizontal scale of the instability is therefore much larger than the Rossby deformation radius. This is in agreement with results from eddy resolving models (McWilliams *et al.*, 1978), where for the CH-case (p 227 of their paper) the Rossby deformation radius is about 36 km and the wavelength of the eddies found is about $400 - 800$ km. The dimensionless angular frequency ω_c is 2.51 giving a dimensional period of the traveling wave of 58 days. If the critical value of β is compared to the actual value of the ACC as in Table 1, it is concluded that the actual ACC is far above critical conditions and therefore highly unstable.

The perturbation streamfunction of the most unstable mode at one phase of the oscillation (at t = 0) and the corresponding potential vorticity perturbation are for both layers shown in Fig. 4; dark (light) shading indicates positive (negative) values. The spatial pattern shows a characteristic 'banana' shape in both layers with maximum amplitude at the center line of the jet. The structure of the zonal velocity of the perturbation therefore has many zeroes in the meridional direction. In upper layer, ϕ_1 and q_1 are out of

phase, whereas there is only a slight phase shift between these quantities in the second layer. There is also a phase shift between ϕ_1 and ϕ_2 characteristic of baroclinic effects in the instability.

Also in McWilliams *et al.* (1978), the linear stability problem was considered for a zonally averaged jet profile. However, no critical conditions were calculated but the growth factors of unstable modes for the actual parameters of the ACC (e.g. as in Table 1). Although the pattern of the most unstable mode is in good qualitative agreement with the patterns they find (compare our Fig. 4 to their Fig. 28), the angular frequency of the traveling wave is a factor 5 smaller. Several factors may cause this difference. First, the traveling wave frequency changes significantly with β as it does for normal Rossby modes. Second, the properties of the mode at criticality may be substantially different from that of the mode with largest growth factor at strong supercriticality. Third, in McWilliams *et al.* (1978) a fixed zonal extent of the domain is considered which allows only for a discrete set of wavenumbers which is a subset of the wavenumbers we consider.

2.3 Finite amplitude development

The linear theory shows that in the case of slightly supercritical control parameter μ, wavelike perturbations with exponentially growing amplitudes will develop. However, this description is only valid in the initial growth stage, where the wave amplitudes are infinitesimally small. To describe the

finite amplitude state, the nonlinear interactions between the various wave components must be taken into account. Further rigorous analysis is possible if the control parameter μ is considered slightly above its critical value μ_c, i.e.

$$\mu = \mu_c + m\epsilon^2 \tag{7a}$$

where

$$\epsilon \ll 1 \quad , \quad m = \mathcal{O}(1) \tag{7b}$$

Because the neutral curve (Fig. 3) can be approximated by a parabola near its minimum, we consider wavenumbers k for which

$$|k - k_c| = \mathcal{O}(\epsilon) \tag{7c}$$

The unstable waves are thus limited to a narrow band around the critical wavenumber k_c. Furthermore, they grow on a timescale which is large compared to the typical wave periods and their modulation is described in new independent variables

$$T = \epsilon^2 t \quad , \quad X = \epsilon(x - c_g t) \tag{7d}$$

where c_g is the group velocity, which is determined by the dispersion relation at criticality. The long spatial scale X is a slow moving coordinate, traveling with the group velocity of the unstable wavepacket.

The finite amplitude of the perturbations will be small compared to that of the basic state, for μ close to μ_c, so the solution vector Φ, now depending on the long space and time variables X and T, is expanded in terms of the small parameter ϵ, Fourier modes of the marginally stable wave $E = exp(i[k_c x + \omega_c t])$ and an amplitude $A(X,T)$ which is undetermined at this stage, i.e.

$$\begin{aligned}
\Phi(x,X,y,t,T) \;&=\; \epsilon A(X,T)\Psi(y)E \\
&+\; \epsilon^2(|A(X,T)|^2\Psi^{(02)}(y) + \; A_X(X,T)\Psi^{(12)}(y)E + \; A^2(X,T)\Psi^{(22)}(y)E^2) \\
&+ \epsilon^3\Phi^{(13)} + \cdots + c.c.
\end{aligned} \tag{7e}$$

The superscripts (ij) refer to wavenumber $i \times k_c$ and $\mathcal{O}(\epsilon^j)$. By substitution of the expansion (7e) into the full equations (3a), the linear stability problem is recovered at $\mathcal{O}(\epsilon E)$. Subsequent analysis (see appendix and for more detail VD97), shows that the evolution of the amplitude $A(X,T)$ is governed by a Ginzburg-Landau equation

$$\frac{\partial A}{\partial T} = \gamma_1 A + \gamma_2 \frac{\partial^2 A}{\partial X^2} - \gamma_3 A|A|^2 \tag{8a}$$

The three complex coefficients γ_i in (8a), as shown in Table 2 for both parameter regimes, depend on all system parameters and are evaluated at criticality $(k = k_c, \mu = \mu_c)$. The coefficients γ_i have been computed numerically, and details on this method are also given in the appendix. For the neutral curve in Fig. 3, it appears that there are no sideband instabilities (see VD97)

in the regime considered here. Hence, the spatially uniform low frequency modulation of the carrier wave, i.e. the Stokes wave

$$A(T) = A_0 e^{i\Omega T}, \tag{8b}$$

which is an exact solution to (8a), is stable to small perturbations. The angular frequency Ω and the amplitude A_0 for the Stokes wave can be readily computed from

$$|A_0|^2 = \frac{Re(\gamma_1)}{Re(\gamma_3)} \; ; \; \Omega = Im(\gamma_1) - Im(\gamma_3)|A_0|^2 \tag{8c}$$

with Re and Im indicating real and imaginary part, respectively. Whereas the linear stability results can be used to determine the transfer of properties from the basic state to perturbations during the instability process, the amplitude of the Stokes wave can be used to investigate the transfer of momentum due to nonlinear interactions of the perturbations.

3 Momentum transfer

3.1 Upgradient momentum transport in the ACC regime

The weakly nonlinear analysis makes the feedback of the interaction of the perturbations and the correction to the basic state explicit. It provides an $\mathcal{O}(\epsilon^2)$ correction to the basic zonal flow through the term $\epsilon^2|A(X,T)|^2\phi_j^{(02)}(y)$ in the expansion (7e) (see equation (A2) in the appendix). The y-dependence

of this correction is determined from

$$r\frac{d^2\phi_j^{(02)}}{dy^2}(y) = -2Re(J(\phi_j, q_j^*)) = -2\ \frac{d}{dy}Re(v_j q_j^*) \tag{9a}$$

where $v_j = ik_c\phi_j$ is the y-structure of the meridional velocity of the most unstable mode, q_j its potential vorticity, and J is the Jacobian as in (3a). Since the zonal flow correction is $u_j^{(02)}(y) = -d\phi_j^{(02)}/dy$, equation (9a) can be written as

$$ru_j^{(02)}(y) = 2Re(v_j q_j^*) \tag{9b}$$

This result indicates that the spatial structure of the meridional potential vorticity flux $v_j q_j^*$ sets the spatial structure of the modification of zonal momentum of the basic state, whereas the amplitude of the correction is measured by the Stokes wave amplitude $|A|^2$. In the absence of friction both terms in (9b) vanish and a higher order expansion in ϵ (cf. (7e)) is needed to capture the modification of the basic state.

To study the interactions in more detail, the equation (9b) can be rewritten in terms of the Reynolds stresses τ_j and the interfacial pressure drag π_d (McWilliams *et al.*, 1978).

$$ru_1^{(02)}(y) = 2Re(v_1 q_1^*) = \frac{d\tau_1}{dy} + F\pi_d \tag{10a}$$

$$ru_2^{(02)}(y) = 2Re(v_2 q_2^*) = \frac{d\tau_2}{dy} - \delta F\pi_d \tag{10b}$$

with π_d and τ_j given by

$$\pi_d = 2|A(X,T)|^2 \; F \; Re(v_1 \phi_2^*) \tag{10c}$$

$$\tau_j = -\overline{u_j v_j} = -2 \; |A(X,T)|^2 \; Re(u_j v_j^*) \tag{10d}$$

where the overbar indicates averaging over one wavelength and use is made of (7e). The Reynolds stresses are plotted in Fig. 5 in both layers for the ACC-case. For $y > 0$ it is found that $\tau_j > 0$ in a region where $d\bar{u}_j/dy < 0$ and hence there is upgradient momentum transport. As $d\bar{u}_j/dy$ is anti-symmetric with respect to $y = 0$, there is also upgradient momentum transport in both layers for $y < 0$.

The spatial structure of the meridional potential vorticity flux $Re(v_j q_j^*)$ is plotted for both layers in Fig. 6. In the upper layer (Fig. 6a), the deceleration of the jet in the center is very small, but strongly increasing at the wing of the jet. If one adds this correction to the basic state (2), one observes that the jet is weakened more at the wings than in the center. In the second layer, the sharpening is obvious from the profile of $Re(v_2 q_2^*)$. The depth averaged zonal velocity correction to the basic state, indicated here by $< Re(vq^*) >$, is given by $< Re(vq^*) >= \frac{r}{2} \int \; u^{(02)} \; dz = \frac{r}{2}(\delta u_1^{(02)} + u_2^{(02)})$ (Fig. 6c) clearly demonstrates the upgradient momentum transport in this case. The vertically averaged jet is sharpened due to the nonlinear interactions of the instabilities.

For both layers, the Reynolds stress and interfacial pressure drag contributions to the momentum transfer are also plotted in Fig. 6. In the upper layer, the deformation of the thermocline by the perturbations gives a negative interfacial pressure drag and decelerates the flow. The negative interfacial pressure drag associated with a change in the slope of the interface leads to an acceleration of the jet in the lower layer. This is easily understood through the thermal wind balance, since a smaller slope of the thermocline leads to a smaller north-south density gradient and consequently to a smaller vertical shear. For both layers, the Reynolds stress divergence tends to accelerate the flow near the center and decelerate near the wings. In the vertically averaged momentum transfer, the interfacial pressure drag cancels since it is an exchange term between both layers. The spatial structure of the upgradient transport is determined by the structure of the divergence of the Reynolds stresses. However, obviously vortex stretching is important to set the shape of these stresses, since it controls the shape of the most unstable mode.

3.2 Regimes of different momentum transport

As downgradient momentum transfer was found in the weakly nonlinear Gulf Stream regime (VD97), it is interesting to investigate the transition from the GS-regime to ACC-regime. The minimum of the neutral curve is traced in the (k, β^{-1})-plane along a path of decreasing F which connects both regimes.

This path is shown in the (F, β)-plane in Fig. 7(a). As F is decreased from its ACC-value, the internal Rossby deformation radius increases, resulting in the selection of smaller wavenumbers of the most unstable mode, as can be seen in Fig. 7(b).

To make a comparison with the ACC-case of the previous section, the streamfunction and potential vorticity perturbation of the dominant mode are shown in Fig. 8 for $F = 13.2$. The spatial patterns of the dominant mode in both regimes are strikingly different, in particular in the wings of the jet. Although the phase difference between ϕ_1 and ϕ_2 and between ϕ and q in both layers is not that different from that in the ACC-regime, the absence of the 'banana' shape is clear. For both layers, the sign of the Reynolds stress divergence (panels (c) and (d) in Fig. 9) is negative in the center of the jet. As a consequence, the perturbation potential vorticity flux $< Re(vq^*) >$, shown together with the potential vorticity gradient of the basic state in Fig. 9, shows a negative value at the center. Hence, for the GS-case downgradient momentum transport occurs since the core of the jet is decelerated and its wings accelerated.

One might expect an exchange of stability along the path of Fig. 7, i.e. the neutral mode in one regime is strongly damped in the other, and an interval exists along the path where both modes coexist but relief one another from being most unstable. However, the GS-mode deforms continuously into the ACC-mode as F is increased. In Fig. 10, the growth rates and frequencies of

the four less damped modes are shown along the connecting path. In Fig. 7 no exchange of stability occurs between modes, but only the pattern of the dominant mode changes along the path.

One way to understand this pattern change is to investigate changes in the mechanical energy balance. For the two–layer model these equations are (Pedlosky, 1987)

$$\frac{\partial E}{\partial t} = I_1 + I_2 + C_p - D \tag{11a}$$

where the total kinetic energy E is given by the sum of kinetic and potential energy over both layers

$$E = \frac{1}{2}\int_{-1}^{1} (\delta(|u_1|^2 + |v_1|^2) + |u_2|^2 + |v_2|^2 + \delta F|\phi_1 - \phi_2|^2)\ dy, \tag{11b}$$

the dissipation D is given by

$$D = \frac{r}{2}\int_{-1}^{1} (\delta(|u_1|^2 + |v_1|^2) + |u_2|^2 + |v_2|^2)\ dy, \tag{11c}$$

and the energy production terms I_1 and I_2 due to Reynolds stresses in both layers are given by

$$\begin{aligned} I_1 &= \int_{-1}^{1} \overline{u}_1(y)\frac{d}{dy}(Re(u_1 v_1^*))\ dy \\ &= \int_{-1}^{1} \overline{u}_1(y)\frac{d\tau_1}{dy}(y)\ dy, \end{aligned} \tag{11d}$$

$$\begin{aligned} I_2 &= \int_{-1}^{1} \overline{u}_2(y)\frac{d}{dy}(Re(u_2 v_2^*))\ dy \\ &= \int_{-1}^{1} \overline{u}_2(y)\frac{d\tau_2}{dy}(y)\ dy. \end{aligned} \tag{11e}$$

Finally, the potential energy conversion C_p is expressed by

$$\begin{aligned} C_p &= \delta F(1-\alpha)\int_{-1}^{1} \overline{u}_1(y) Re(-v_1\phi_2^*)\ dy \\ &= -\delta(1-\alpha)\int_{-1}^{1} \overline{u}_1(y)\pi_d(y)\ dy \end{aligned} \tag{11f}$$

The net energy term $\partial E/\partial t = Re(\sigma)E$ is zero since $Re(\sigma) = 0$ along the path of the dominant mode in Fig. 7. Consequently, the energy balance for this mode reads

$$D = C_p + I_1 + I_2. \tag{12}$$

The terms in this energy balance for the most unstable mode are plotted in Fig. 11 as a function of F along the path connecting the regimes. Starting from small values of F, the instability is dominated by barotropic effects, indicated by the balance between D and I_1. As F is increased, the baroclinic contribution to the instability C_p becomes more important, eventually dominating the right hand side of (12). Near $F = 13.5$, I_1 changes sign, indicating a transition from a regime where Reynolds stresses extract kinetic energy from the mean state ($I_1 > 0$ for $F < 13.5$) to a regime where the energy transfer due to horizontal shear is back to the basic state.

This is in agreement with the change in pattern of the unstable mode with F. The strong curvature near the wings of the mode in the ACC-regime, with isolines of the perturbation streamfunction leaning against the mean flow, acts to decelerate the basic state (Pedlosky, 1987). Note that

when the integral quantity I_1 is negative, there is still a mixed instability, since locally the Reynolds stress is still destabilizing.

From $F \approx 27$ onward, it appears that the center of the jet is accelerated and upgradient transport is encountered. The perturbation potential vorticity flux has already the same shape as in the ACC-regime. The interval from $F = 13.5$ to 27 is a transition region, in which the value of the minimum of $< Re(vq^*) >$ increases and becomes positive with increasing F. The role of baroclinic effects is evident from the increase of C_p, i.e. a sufficient large value of F is needed to obtain upgradient transport. In a completely barotropic context, upgradient transport is impossible, since only instabilities through horizontal shear are possible, having a positive I_1 (extracting energy from the basic state) balancing the dissipative effects D. Baroclinic processes in the unstable mode extract energy from the mean state, whereas horizontal shear effects take care of the input of energy back into the mean state.

4 Discussion

Within a two-layer quasi-geostrophic model on a midlatitude β-plane, the finite amplitude evolution of mixed barotropic/baroclinic instabilities on an eastward zonal jet was studied. The amplitude of the most unstable mode is determined by equilibration due to nonlinear effects. An example of mean upgradient momentum transport due to nonlinear equilibration of mixed instabilities is found. Although this case is not directly relevant to the actual

ACC which is far above supercriticality, it serves as a clear example of how upgradient momentum transport is accomplished.

It is interesting to look at the energy transfer between mean state and perturbations as in McWilliams *et al.* (1978) at slightly supercritical conditions. To divide the flow into a mean component $< \Phi >$ and a deviation from the mean state Φ' (which is zero when averaged over a typical oscillation period of an unstable wave) we would have to write our expansion (7e) as

$$< \Phi > = \bar{\Psi} + \epsilon^2 \Phi^{(02)} + \cdots \tag{13a}$$

$$\Phi' = \epsilon \Phi^{(11)} E + \epsilon^2 (\Phi^{(12)} E + \Phi^{(22)} E^2) + \epsilon^3 \Phi^{(13)} E + \cdots + c.c. \tag{13b}$$

where $\bar{\Psi}$ is the streamfunction vector corresponding to the basic state velocity profile (2). The important point is that the $\Phi^{(02)}$ contribution depends on the slow time and space scales X and T. Hence, this decomposition shows that the energy and momentum transfer from nonlinear interactions back to the basic state occurs on a much longer time scale (in the weakly nonlinear regime) then a typical wave period.

A mechanistic picture of the physics of upgradient momentum transport is obtained from an interpretation of the equations which show the basic state correction due to the nonlinear interactions of the most unstable modes. These modes have a structure as in Fig. 4, and the particular mode is most unstable because it is able to extract in an optimal way energy out of the basic state (see e.g. Pedlosky (1987)). In fact, there are two such waves, traveling

in opposite directions. Equation (9a) shows that this interaction induces a potential vorticity flux which leads to changes in the relative vorticity of the basic zonal flow. This potential vorticity flux is composed of a Reynolds stress contribution and a contribution due to the deformation of the interface separating both layers. The interfacial pressure drag gives no contribution to the vertically averaged momentum transfer so that the Reynolds stress contribution reflects the upgradient momentum transfer.

Note, however, that vortex stretching is essential to obtain this particular Reynolds stress distribution. This can be seen from the terms in the mechanical energy balance (12) which are followed along a path connecting GS-regime and ACC-regime. Only when the baroclinic conversion term becomes large enough, then the Reynolds stress contribution can be negative and still dissipation is balanced. This boundary occurs already at intermediate F, and certainly at acceptable values of the validity of quasi-geostrophic theory.

The modification of the zonal jet is due to the self-interaction of a single dominant mode as it is now set by the $\mathcal{O}(\epsilon^2)$ balance in the expansion of the mean field variables. This is in agreement with the theory as described in Rhines and Holland (1979) but makes it much more explicit by providing a mechanism for the potential vorticity flux, i.e. the self interaction. To show this in more detail, we consider the depth integrated acceleration of the zonal jet due to the interaction of eddy - fluxes as derived in their paper

for a continuously stratified flow, i.e.

$$\frac{\partial}{\partial t}\int < u > dz = \int < v'q' > dz \tag{14a}$$

The inclusion of linear friction implies a substitution

$$\frac{\partial}{\partial t} \rightarrow \frac{\partial}{\partial t} + r$$

and yields

$$\int (\frac{\partial}{\partial t} + r) < u > dz = \int < v'q' > dz \tag{14b}$$

Substitution of the expressions for the mean and eddy fields (11) results, in terms of our two-time scale expansion (7c), in a modification of the jet $u^{(02)}$ at $\mathcal{O}(\epsilon^2)$ by

$$r\int u^{(02)}dz = 2Re\int vq^* dz \tag{14c}$$

which reduces for a two-layer model to the expressions (9b) found above.

In the inviscid limit ($r = 0$), the $\mathcal{O}(\varepsilon^2)$ correction to the basic state vanishes. This can be demonstrated by writing $v = |v|e^{i\eta}$ and $q = |q|e^{i\zeta}$ where η and ζ are the arguments of these quantities. The potential vorticity flux can then be expressed as

$$Re(vq^*) =\mid v \mid\mid q \mid cos(\eta - \zeta) \tag{15}$$

which shows that the difference in the argument determines whether the interaction will have non-zero amplitude. In the absence of friction, at critical

conditions, the meridional structures of potential vorticity and streamfunction are in phase and, with $v = ik_c\psi$, we find that $\eta - \zeta$ is a multiple of $\pi/2$ and hence the potential vorticity flux (15) vanishes. In this case, equation (14c) is trivially satisfied and the momentum transport has to be determined from higher order (and much more complicated) analysis. With $\mathcal{O}(1)$ linear friction, the $\mathcal{O}(\varepsilon^2)$ correction does not vanish. The frictional terms in the (two-layer) model allow one therefore to determine the amplitude of the correction through the Ginzburg - Landau equation (8a).

For the maintanance of idealized eastward jets, the upgradient momentum transport appears to be a relevant feature and the weakly nonlinear approach as used here seems capable of capturing its main features.

Appendix: Derivation of the reduced model

In this appendix the derivation of the equation that governs the evolution of the amplitude $A(X,T)$ in (7e) is presented. After substitution of (7) into (3a) terms of like orders in ϵ and E are collected. At $\mathcal{O}(\epsilon E)$ the linear stability problem is encountered

$$(i\omega_c\hat{\mathcal{M}}(k)+\hat{\mathcal{L}}(k))\Psi=0 \tag{A.1}$$

where the operators $\hat{\mathcal{M}}(k)$ and $\hat{\mathcal{L}}(k)$, for the two-layer QG model, are given by

$$\hat{\mathcal{M}}(k)=\begin{pmatrix}\frac{d^2}{dy^2}-k^2-F & F\\ \delta F & \frac{d^2}{dy^2}-k^2-\delta F\end{pmatrix}$$

and

$$\hat{\mathcal{L}}(k)=$$

$$\begin{pmatrix}(ik\overline{u}_1+r)(\frac{d^2}{dy^2}-k^2)-ik(\overline{u}_1F-\overline{\Pi}_1') & ik\overline{u}_1F\\ ik\overline{u}_2\delta F & (ik\overline{u}_2+r)(\frac{d^2}{dy^2}-k^2)-ik(\delta\overline{u}_2F+\overline{\Pi}_2')\end{pmatrix}.$$

and ω_c is the angular frequency of the neutral mode.

At $\mathcal{O}(\epsilon^2)$ and at $\mathcal{O}(\epsilon^2E^2)$ two invertible problems describe the nonlinear self-interaction of the marginally stable wave. This results in a modification of the basic state and a second harmonic contribution given by $\Psi^{(02)}$ and $\Psi^{(22)}$, respectively, which satisfy

$$\hat{\mathcal{L}}(0)\Psi^{(02)}=-2Re(\mathcal{N}(\Psi)\Psi^*) \tag{A.2}$$

$$(2i\omega_c\hat{\mathcal{M}}(2ik_c) + \hat{\mathcal{L}}(2ik_c))\Psi^{(22)} = -\mathcal{N}(\Psi)\Psi \qquad (A.3)$$

where Re indicates real part, $*$ the complex conjugate and the nonlinear operator $\mathcal{N}$ is defined as,

$$\mathcal{N}(\Psi) =$$

$$\begin{pmatrix} (\frac{\partial\phi_1}{\partial x}\frac{\partial}{\partial y} - \frac{\partial\phi_1}{\partial y}\frac{\partial}{\partial x})(\nabla^2 - F) & F(\frac{\partial\phi_1}{\partial x}\frac{\partial}{\partial y} - \frac{\partial\phi_1}{\partial y}\frac{\partial}{\partial x}) \\ \delta F(\frac{\partial\phi_2}{\partial x}\frac{\partial}{\partial y} - \frac{\partial\phi_2}{\partial y}\frac{\partial}{\partial x}) & (\frac{\partial\phi_2}{\partial x}\frac{\partial}{\partial y} - \frac{\partial\phi_2}{\partial y}\frac{\partial}{\partial x})(\nabla^2 - \delta F). \end{pmatrix}$$

These equations are complemented with the appropriate boundary conditions at this order in the expansion. The groupvelocity c_g appears as a solvability condition at $\mathcal{O}(\epsilon^2 E)$

$$(i\omega_c\hat{\mathcal{M}}(k_c) + \hat{\mathcal{L}}(k_c))\Psi^{(12)} = -(\hat{\mathcal{L}}_k(k_c) + i\omega_c\hat{\mathcal{M}}_k(k_c) - c_g\hat{\mathcal{M}}(k_c))\Psi, \qquad (A.4)$$

where a subscript indicates differentiation of the operator with respect to the indicated parameter. From differentiation of the eigenvalue problem and inspection of the right hand side of equation (A.4) it is observed that the solution $\Psi^{(12)}$ and the group velocity are given by

$$\Psi^{(12)} = -i\frac{\partial\Psi}{\partial k} \qquad \text{and} \qquad c_g = \frac{\partial\omega}{\partial k}$$

both evaluated at criticality. Since the linear operator in the lefthandside is identical to the linear stability operator, the solution at this order is determined up to the addition of the homogeneous solution of $(A.4)$, which is omitted here as it does not appear in the amplitude equation (7e). At

$\mathcal{O}(\epsilon^3 E)$ a singular problem is obtained for which the righthand side now depends explicitly on the amplitude $A(X,T)$ and the vectors Ψ , $\Psi^{(12)}$, $\Psi^{(02)}$ and $\Psi^{(22)}$, i.e.

$$(i\omega_c\hat{\mathcal{M}}(k_c)+\hat{\mathcal{L}}(k_c))\Phi^{(13)} = -(\hat{\mathcal{M}}(k_c)\Psi\frac{\partial A}{\partial T}+m\mathbf{\Gamma}A+\mathbf{\Sigma}\,\frac{\partial^2 A}{\partial X^2}+\mathbf{\Lambda}\,A|A|^2) \quad (A.5)$$

where

$$\begin{aligned}
\mathbf{\Gamma} &= (\hat{\mathcal{L}}_\mu(k_c) - i\omega_c\hat{\mathcal{M}}_\mu(k_c))\Psi, \\
\mathbf{\Sigma} &= \frac{1}{2}(i\omega_c\hat{\mathcal{M}}_{kk}(k_c) - \hat{\mathcal{L}}_{kk}(k_c) - 2c_g\hat{\mathcal{M}}_k(k_c))\Psi \\
&\quad + i(i\omega_c\hat{\mathcal{M}}_k(k_c) - c_g\hat{\mathcal{M}}(k_c) - \hat{\mathcal{L}}_k(k_c))\Psi_k
\end{aligned}$$

and the vector $\mathbf{\Lambda}$ contains all nonlinear interactions at this order

$$\mathbf{\Lambda} = \mathcal{N}(\Psi)\Psi^{(02)} + \mathcal{N}(\Psi^{(02)})\Psi + \mathcal{N}(\Psi^{(22)})\Psi^* + \mathcal{N}(\Psi^*)\Psi^{(22)}$$

In general, the right hand side of $(A.5)$ is not contained in the range of $i\omega_c\hat{\mathcal{M}} + \hat{\mathcal{L}}$. On an $\mathcal{O}(\epsilon^{-2})$ timescale, valid solutions to $(A.5)$ are possible if the righthand side is orthogonal to the kernel of the linear operator. This so called solvability condition is a direct result of the Fredholm alternative. Since the kernel of this operator has dimension 1, it is spanned by 1 vector, say $\mathbf{Q}$, which implies that $\mathbf{Q}^H(i\omega_c\hat{\mathcal{M}} + \hat{\mathcal{L}})\mathbf{W} = 0$ under the appropriate innerproduct, where $\mathbf{W}$ is an arbitrary vector and H indicates Hermitian transposed.

The amplitude equation resulting from the solvability condition for $(A.5)$

is called the Ginzburg-Landau equation :

$$\frac{\partial A}{\partial T} = \gamma_1 A + \gamma_2 \frac{\partial^2 A}{\partial X^2} - \gamma_3 A|A|^2 \tag{A.6}$$

where the three coefficients γ_j, all evaluated at criticality ($k = k_c, \mu = \mu_c$), are given by

$$\gamma_1 = m\frac{\mathbf{Q}^H \mathbf{\Gamma}}{\mathbf{Q}^H \hat{\mathcal{M}} \Psi} = m\frac{\partial \sigma}{\partial \mu}$$
$$\gamma_2 = \frac{\mathbf{Q}^H \mathbf{\Sigma}}{\mathbf{Q}^H \hat{\mathcal{M}} \Psi} = -\frac{1}{2}\frac{\partial^2 \sigma}{\partial k^2}$$
$$\gamma_3 = -\frac{\mathbf{Q}^H \mathbf{\Lambda}}{\mathbf{Q}^H \hat{\mathcal{M}} \Psi}$$

For the zonal jet these coefficients have to be calculated numerically, since the linear stability problem cannot be analytically. To reduce the two-point boundary value problem ($A.1$) to an algebraic eigenvalue problem a pseudo spectral method is used. The solutions are expanded in a cosine-series, symmetric with respect to $y = 0$, which already satisfy the boundary conditions. The collocation points are given by

$$y_i = \frac{2i-1}{2N+1} \ ; \ i = 1, ..., N, \tag{A.7}$$

where we take advantage of the symmetry of the problem, solving only for $y > 0$. Expanding the eigenfunctions of the linear stability problem into the basisfunctions and applying the two-point eigenvalue problem at the collocation points ($A.7$) leads to a generalized $2N$-dimensional eigenvalue problem of the form

$$(\hat{\mathbf{M}}\ \sigma + \hat{\mathbf{L}})\hat{\Psi} = \mathbf{0},$$

where $\hat{\Psi}$ is the discretized equivalent of Ψ in (6a). For the results presented here, the cosine-series has been truncated at $N = 71$, which provided sufficient accuracy of both the eigenvalues and the eigenvectors, as well as the coefficient γ_3 for the nonlinear term in the Ginzburg-Landau equation.

References

Eckhaus, W. (1965). *Studies in nonlinear stability theory.* Springer Verlag.

Held, I. (1975). Momentum transport by geostrophic eddies. *J. Atm. Sc.*, **32**, 1494–1497.

Hoskins, B. J. and Valdes, P. J. (1990). On the existence of storm-tracks . *J. Atm. Sc.*, **47**, 1854–1864.

Kuo, H. (1951). The general circulation and the stability of zonal flow. *Tellus*, **3**, 268–284.

Marshall, J., Olbers, D., Ross, H., and Wolf-Gladrow, D. (1993). Potential vorticity constraints on the dynamics and hydrography of the Southern Ocean. *J. Phys. Ocean.*, **23**, 465–487.

McWilliams, J., Holland, W., and Chow, J. (1978). A description of numerical Antarctic Circumpolar Currents. *Dyn. Oc. Atm.*, **2**, 213–291.

Nowlin, W. and Klinck, J. (1986). The physics of the Antarctic Circumpolar Current. *Rev. Geophys. Space Phys.*, **24**, 469–491.

Pedlosky, J. (1963). Baroclinic instability in two-layer systems. *Tellus*, **15**, 20–25.

Pedlosky, J. (1970). Finite amplitude baroclinic waves. *J. Atm. Sc.*, **27**, 15–30.

Pedlosky, J. (1987). *Geophysical Fluid Dynamics 2nd. ed.* Springer Verlag.

Rhines, P. B. and Holland, W. R. (1979). A theoretical discussion of eddy-driven mean flows. *Dyn. Oc. Atm.*, **3**, 289–325.

Romea, R. D. (1977). The effects of friction and β on finite amplitude baroclinic waves. *J. Atm. Sc.*, **34**, 1689–1695.

Van der Vaart, P. and Dijkstra, H. (1997). Sideband instabilities of mixed barotropic/ baroclinic waves growing on a midlatitude zonal jet. *Phys. Fluids*, **9**, 615–631.

parameter	ACC	GS
α	0.22	0.22
F	300.0	13.2
δ	0.22	0.22
β	28.0	0.22
r	0.2	0.2
ν	0.5	0.5

Table 1: *Standard values of the parameters. The value of β is the actual value for both regimes.*

coefficient	ACC	GS
γ_1	$4.519\ 10^{-2} + i\ 8.512\ 10^{-3}$	$1.236\ 10^{-1} - i\ 8.549\ 10^{-2}$
γ_2	$7.895\ 10^{-2} + i\ 1.029\ 10^{-1}$	$2.493\ 10^{-1} + i\ 2.540\ 10^{-2}$
γ_3	$1.088\ 10^{4} + i\ 6.092\ 10^{3}$	$2.267 - i\ 7.255$

Table 2: *The coefficients γ_i in the Ginzburg-Landau equation* (8a) *for both regimes.*

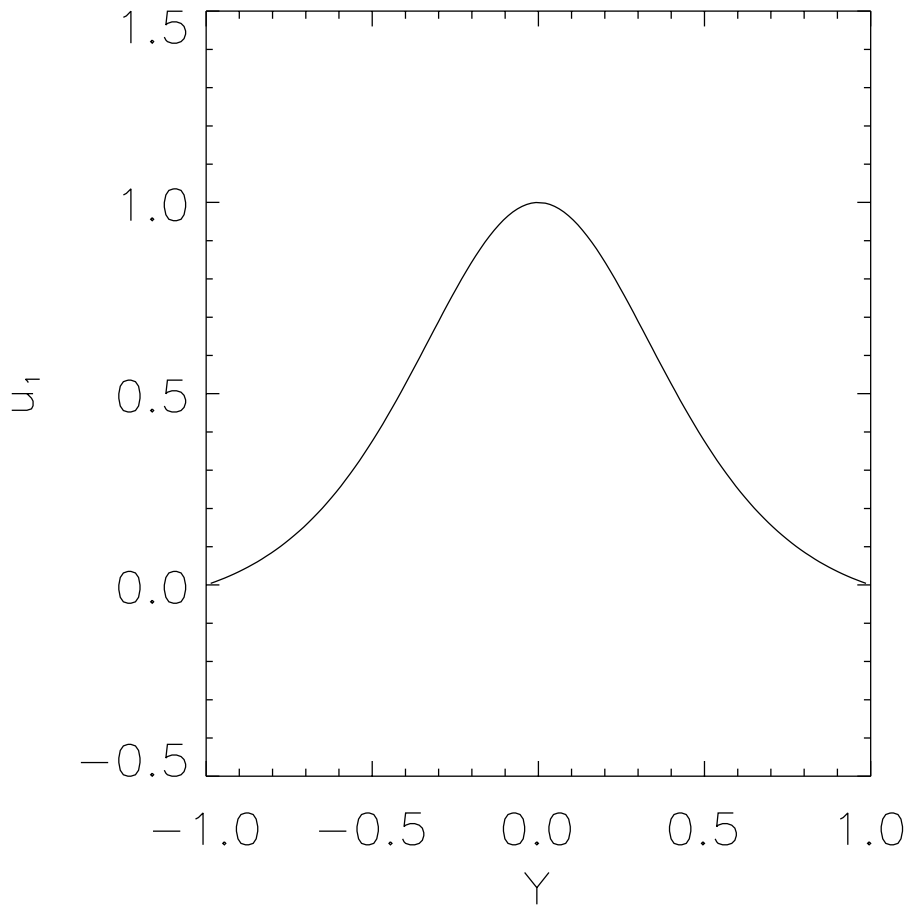

Figure 1: *Zonal velocity profile* $\overline{u}_1$ *of the basic state.*

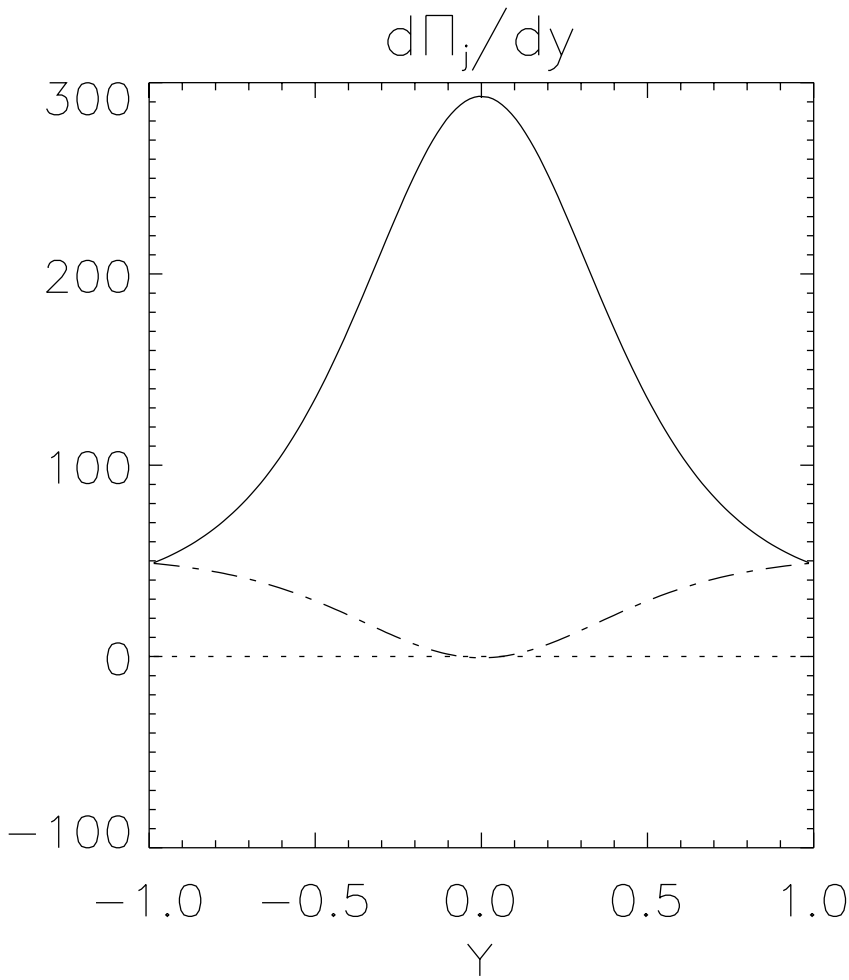

Figure 2: *Potential vorticity gradient of the basic state in layer 1 (solid) and in layer 2 (dash-dotted) (ACC case).*

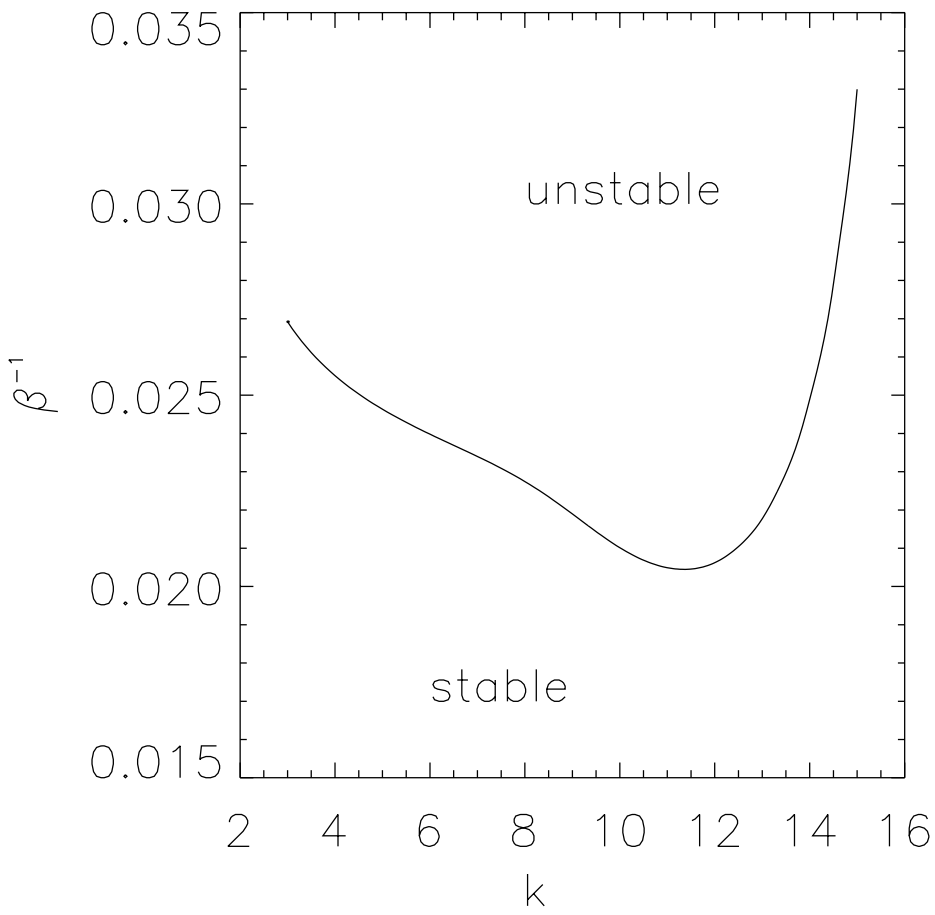

Figure 3: *Neutral curve for the parameter values of the ACC regime and* β^{-1} *as control parameter.*

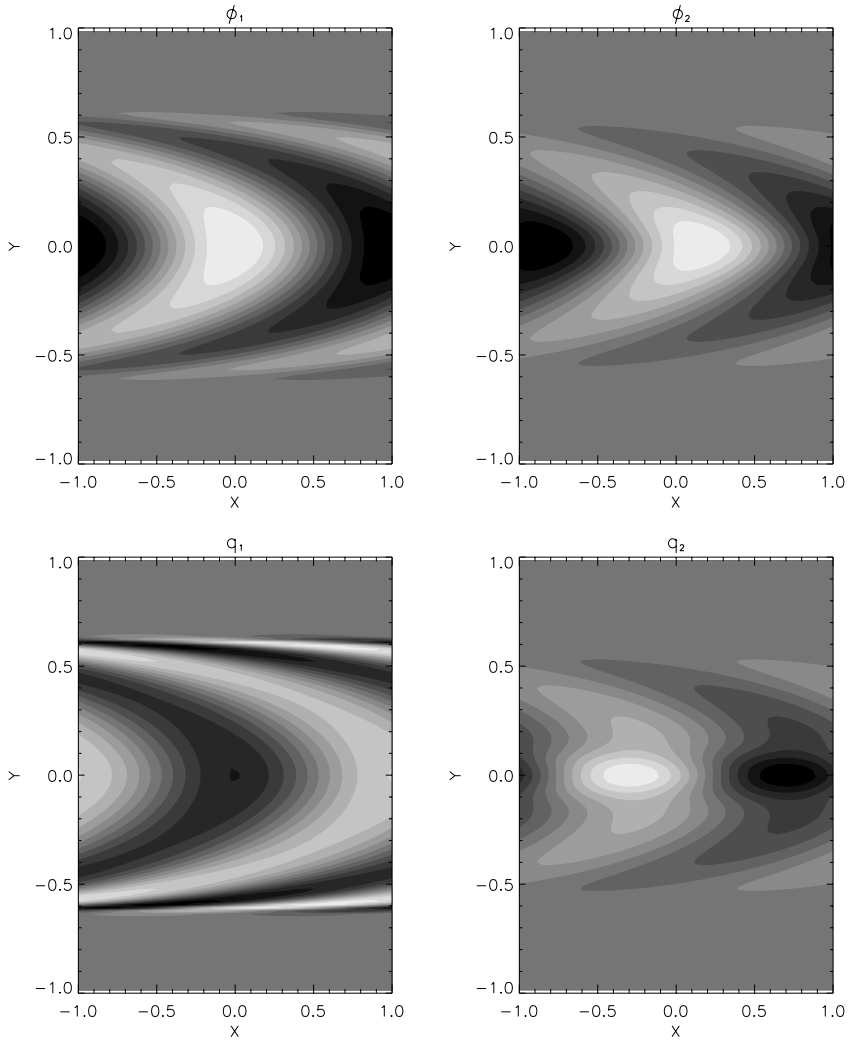

Figure 4: *Perturbation streamfunctions ϕ of the most unstable mode at neutral conditions (at the minimum of the curve in Fig. 3 in layer 1 (ϕ_1) and layer 2 (ϕ_2) (ACC regime). Corresponding potential vorticity perturbations for layer 1 (q_1) and layer 2 (q_2) are also plotted. Dark (light) shading indicates positive (negative) values.*

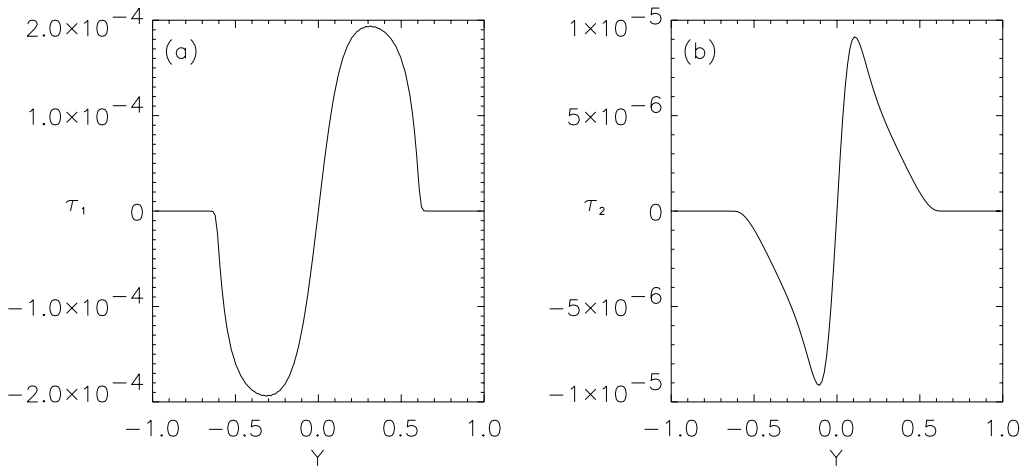

Figure 5: *The Reynolds stresses τ_j due to the interaction of the unstable modes in both layers (ACC regime) as defined in eq.* (10d)

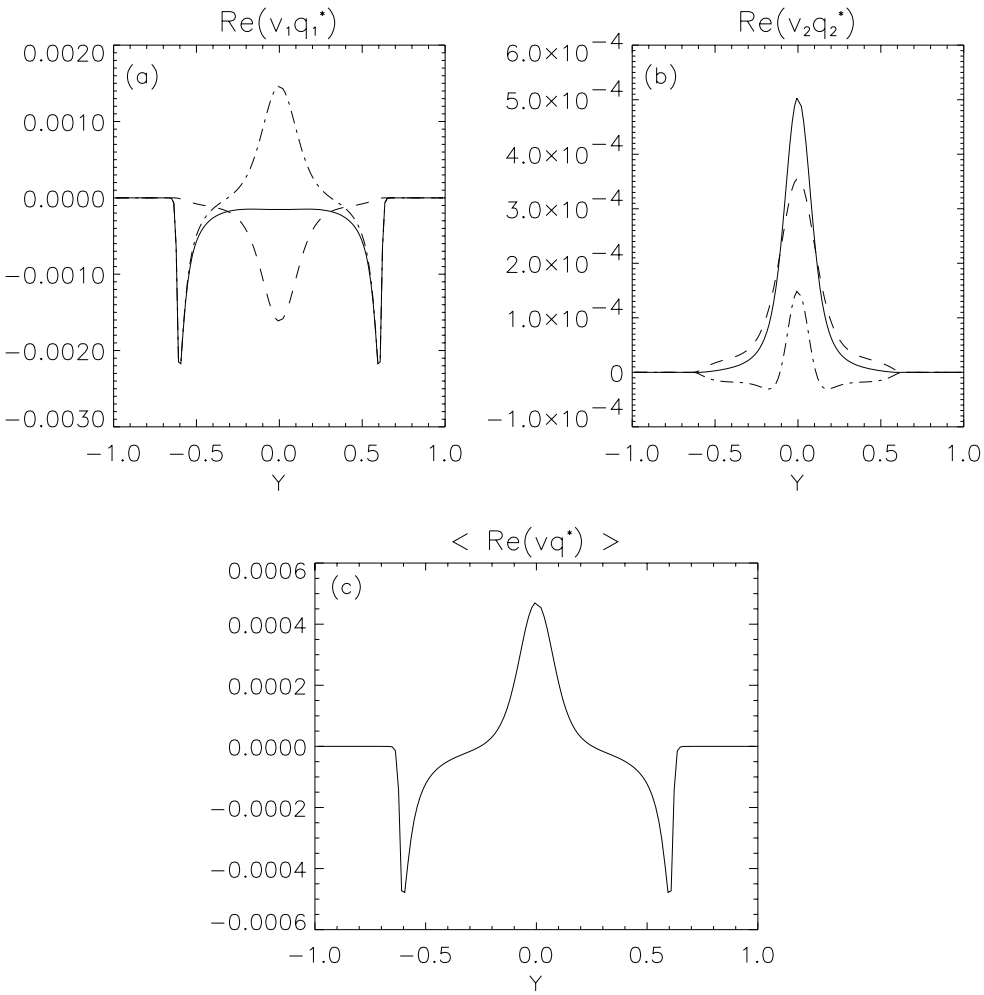

Figure 6: *The spatial structure of the potential vorticity flux (drawn line) and its decomposition into Reynolds stress divergence (τ'_j, dashed) and interfacial pressure drag (π_d, dash-dotted) in layer 1 (a) and layer 2 (b).(c) The vertically averaged zonal velocity correction.*

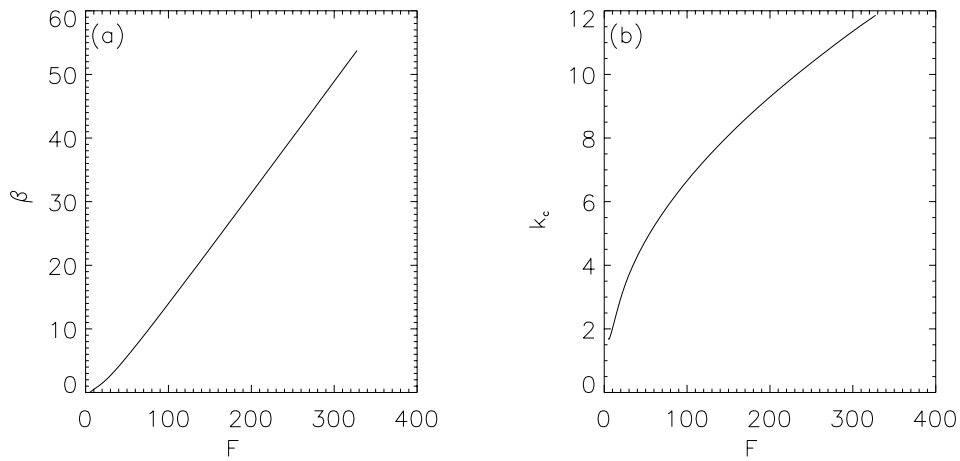

Figure 7: *(a). The path in the (F, β)-plane connecting the Gulf Stream parameter regime to the ACC regime. Each point on the line corresponds to a minimum of the neutral curve. (b). The wave number dependence of the most unstable wave as a function of F, along the path of (a).*

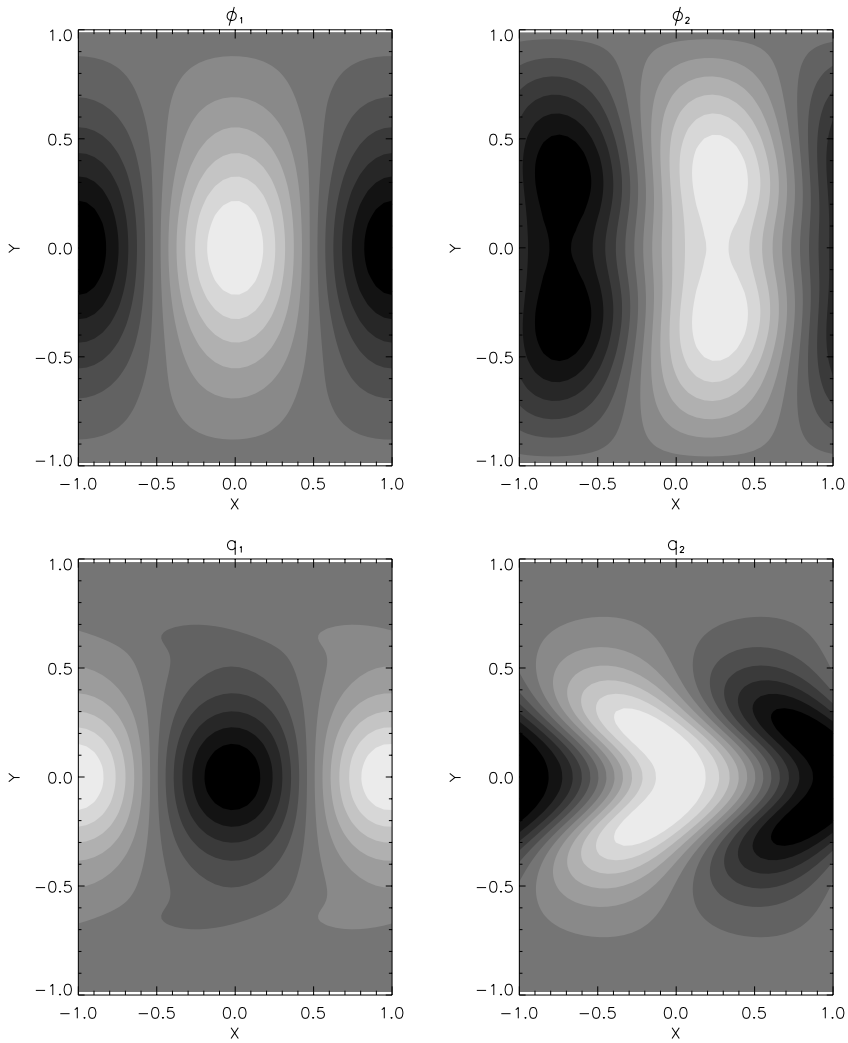

Figure 8: *Perturbation streamfunctions of the most unstable mode at neutral conditions in layer 1 (ψ_1) and layer 2 (ψ_2) (Gulf Stream regime). Corresponding potential vorticity functions in layer 1 (q_1) and layer 2 (q_2). Color coding as in Fig. 4.*

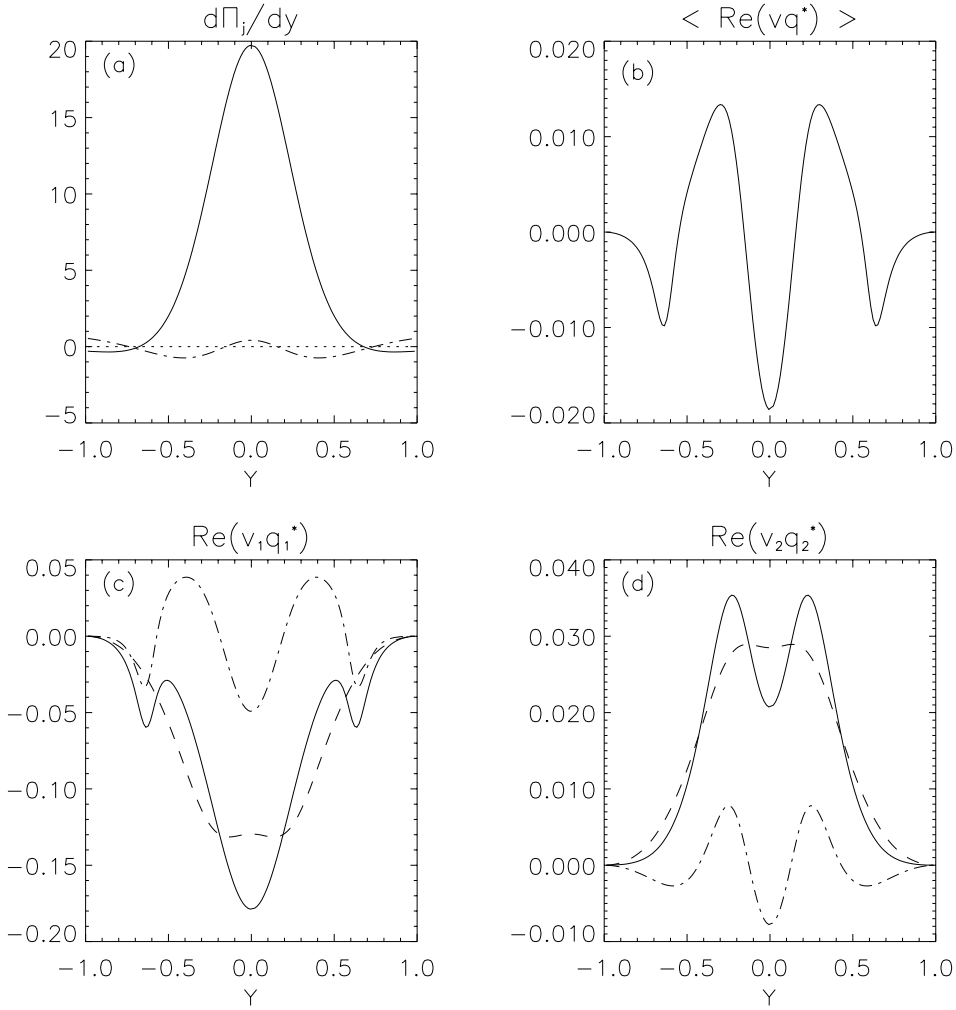

Figure 9: *(a) Potential vorticity gradient of the basis state in layer 1 (solid) and in layer 2 (dash-dotted) for* $F = 13.2$ *(Gulf Stream regime). (b) The vertically averaged zonal velocity correction. (c), (d) The spatial structure of the potential vorticity flux (drawn line) and its decomposition into Reynolds stress divergence (* τ'_j*, dashed) and interfacial pressure drag (*π_d*, dash-dotted) in layer 1 (c) and layer 2 (d).*

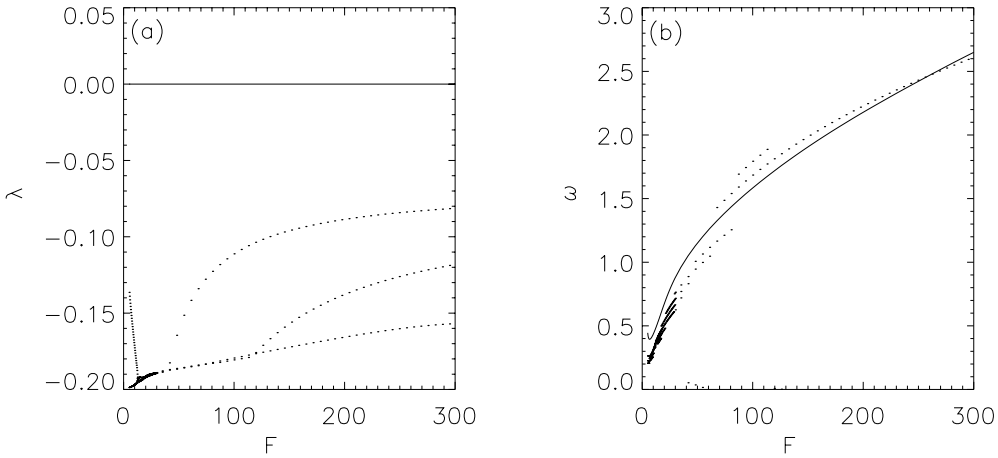

Figure 10: *(a). The growth rates of the four less damped eigenvalues along the path in Fig. 7. The drawn line at* $\lambda = 0$ *indicates the neutral mode. (b). The frequencies of the four less damped eigenvalues along the path in Fig. 7. The drawn line indicates the frequency of the neutral mode.*

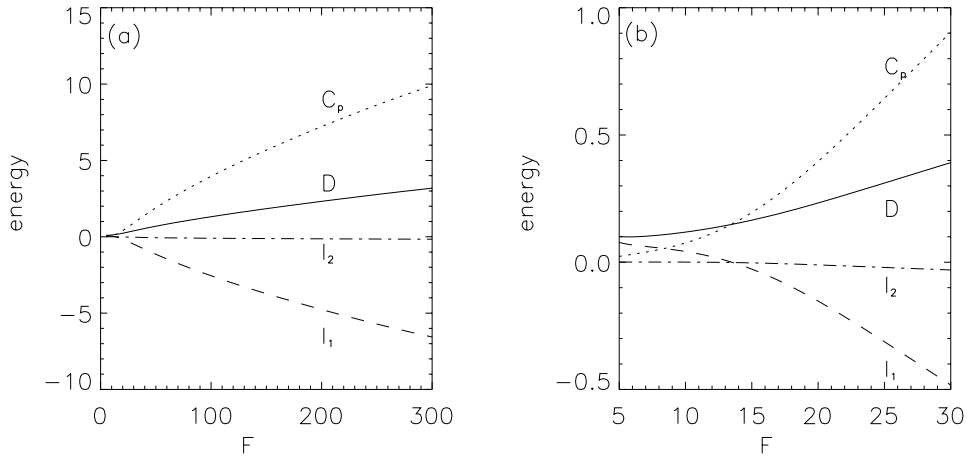

Figure 11: *(a). Terms of the mechanical energy balance along the path shown in Fig. 7. The four terms are dissipation (D), conversion of potential energy (C_p), Reynolds stress conversion in layer 1 (I_1) and 2 (I_2). (b). Close up of (a) near the Gulf Stream regime.*